JACS
JOURNAL OF THE AMERICAN CHEMICAL SOCIETY
Article
pubs.acs.org/JACS

Differentially Addressable Cavities within Metal–Organic Cage-Cross-Linked Polymeric Hydrogels

Jonathan A. Foster,[†] Richard M. Parker,[†] Ana M. Belenguer,[†] Norifumi Kishi,[‡] Sam Sutton,[†] Chris Abell,[†] and Jonathan R. Nitschke*,[†]

[†]University of Cambridge, Lensfield Road, Cambridge, CB2 1EW, United Kingdom
[‡]Chemical Resources Laboratory, Tokyo Institute of Technology, 4259 Nagatuta, Midori-ku, Yokohama 226-8502, Japan

Supporting Information

ABSTRACT: Here we report a new class of hydrogels formed by polymers that are cross-linked through subcomponent self-assembled metal–organic cages. Selective encapsulation of guest molecules within the cages creates two distinct internal phases within the hydrogel, which allows for contrasting release profiles of related molecules depending on their aptitude for encapsulation within the cages. The hydrogels were fabricated into microparticles via a droplet-based microfluidic approach and proved responsive to a variety of stimuli, including acid and competing amine or aldehyde subcomponents, allowing for the triggered release of cargo.

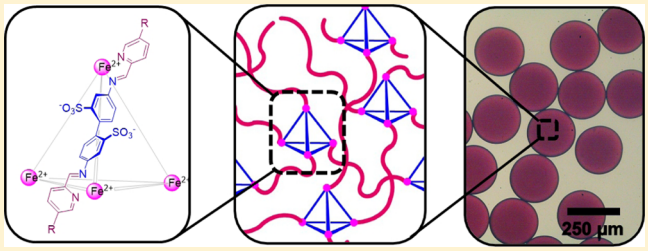

INTRODUCTION

The controlled release of molecules in response to stimuli or over time is important in a wide range of technologies including the delivery of pharmaceuticals, fragrances, flavorings, detergents, cosmetics and fertilizers.[1−5] The rate of release is typically governed by dissolution, diffusion, swelling, partitioning or erosion mechanisms, which may be triggered or accelerated in response to stimuli.[6−9] An alternative recent approach is to incorporate chemical functionalities that selectively bind to the species being released, providing further control over its release profile.[10] A variety of such affinity-based delivery systems have been developed that utilize electrostatic interactions, hydrogen bonding and hydrophobic interactions, including the host–guest chemistry of macrocycles.[10−12] Here we report a new class of polymeric hydrogels, in which cross-links are formed by metal–organic cages. These hydrogels are able to selectively encapsulate guest molecules, allowing for differential release profiles of closely related molecules from within two distinct kinds of spaces within the hydrogels—both the pores within the hydrogel, and the inner phases of the cages, show distinct guest uptake, release, and selectivity properties. Triggered release from these differentiated spaces can also be achieved in response to a variety of external stimuli.

Metal–organic cages are a diverse class of self-assembled structures that possess internal cavities able to selectively encapsulate guest molecules.[13−19] These cages are useful in a range of sensing,[20,21] storage,[22] separation,[23] delivery[24] and catalysis applications.[25−27] A recent approach to assembling cages involves the metal-templated condensation of amine and 2-formylpyridine subcomponents to form dynamic imine bonds, which are stabilized against hydrolysis by coordination to the template.[28,29] The reversibly-formed nature of the linkages provides an error-checking process that allows the system to converge to a thermodynamically favorable structure.[30,31] We and others have used this approach to create a diverse array of metal–organic cages of different sizes and shapes, with cavities capable of binding a variety of guests.[28,30]

Polymeric supramolecular hydrogels can be formed by cross-linking soluble polymers through noncovalent interactions to form a matrix, which immobilizes the surrounding solvent through surface tension, giving rise to the gel phase.[32,33] The ability of supramolecular gels to trap large numbers of molecules within the pores of their matrices makes them useful for applications that include drug delivery,[9,32] wound healing,[34,35] crystallization[36] and catalysis.[37,38] Microparticles formed from supramolecular gels can be mass produced with uniform size, which makes them ideal for delivery applications.[39−43]

Different interactions have been employed to create supramolecular gels, including coordination to metal cations[39,44,45] and anions,[46] dynamic-covalent bonds,[47] hydrophobic interactions,[48] host–guest interactions[5,49−51] and hydrogen bonding.[33,52] The dynamic nature of the bonding in these systems gives rise to useful properties that include self-healing,[47] shear thinning[53] and stimuli-responsive behavior.[48,54] Only a few gels formed by metal-templated imine formation have been reported, including an organogel formed from low molecular weight complexes reported by Kolehmainen and co-workers[55] and heat-set gelation in a series of dynamic-covalent metallopolymers.[56,57]

Cage **1** (Figure 1, R = H) is readily formed from commercially available starting materials under ambient conditions in water.[58−60] We hypothesized that by functionaliz-

Received: June 1, 2015
Published: July 8, 2015

DOI: 10.1021/jacs.5b05507
J. Am. Chem. Soc. 2015, 137, 9722−9729

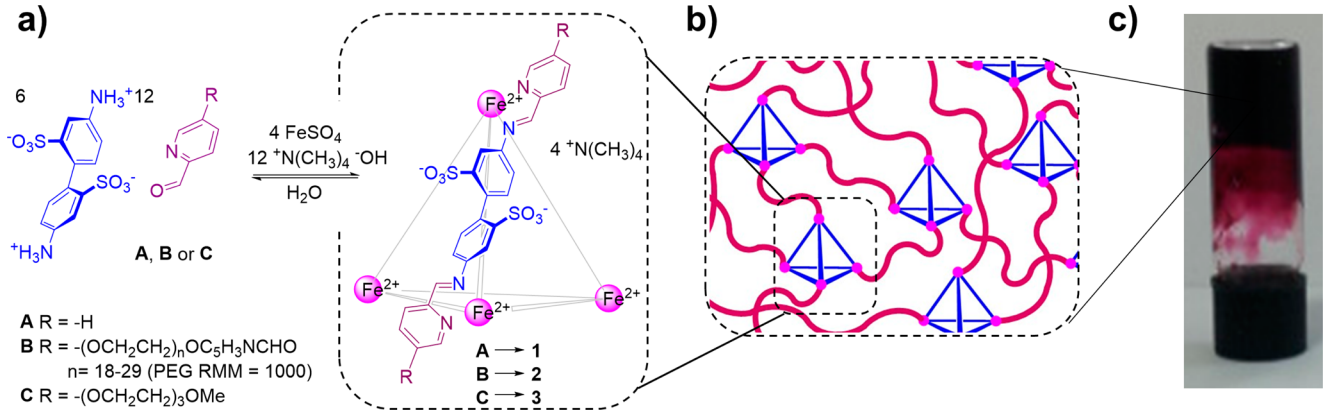

Figure 1. Metal–organic cage cross-linked hydrogel formation: (a) synthesis of cages **1**–**3** using aldehydes **A**–**C**, and (b) a schematic view of the structure of the cage-cross-linked gel. (c) A photograph showing an inverted vial containing a 15 wt % hydrogel formed by cage **2**.

ing water-soluble polymers with cage-forming subcomponents, cage assembly would result in cross-linking of the polymers, triggering hydrogel formation. The combination of strong-but-reversible imine and coordination bonds was expected to create robust, yet responsive and tunable, gel systems. In addition to cross-linking the polymers to give rise to hydrogels, we anticipated that the metal–organic cages would impart the hydrogels with the ability to selectively bind certain guests within spaces distinct from the gel pores.

Hydrogel Synthesis and Characterization. Polyethylene glycol (PEG) with an average molecular weight (M_n) of 1000 g mol^{-1} was functionalized with 2 equiv of 5-fluoro-2-formylpyridine to generate subcomponent **B**, as described in the Supporting Information Section 1.2. Comparison of the integrals for the aromatic protons in the ^{1}H NMR spectrum with those for the ethylene glycol chain gave a ratio of 1:44, corresponding to the expected average molecular weight of the PEG chains (Figure S1). Mass spectrometry confirmed the presence of a doubly functionalized polymer with masses corresponding to PEG chains containing 18–29 repeat units.

The cage-cross-linked polymer network (Figure 1b) was generated by mixing an aqueous solution of dialdehyde **B** (6 equiv), 4,4′-diaminobiphenyl-2,2′-disulfonic acid (6 equiv) and tetramethylammonium hydroxide (12 equiv) with an aqueous solution of iron(II) sulfate heptahydrate (4 equiv). When 15% by weight (15 wt %) of building blocks were used, a purple color was observed immediately upon mixing, which indicated the formation of an iron complex, and within 1 min the sample no longer flowed within its container, indicating hydrogel formation (Figure 1c).

The presence of a hydrogel was confirmed by rheometry. An elastic modulus (G') of 10^6 Pa was measured, an order of magnitude higher than the viscous modulus (G'') with a linear response observed over a wide range of frequencies (0.1–100 Hz, Figure S3). A strain sweep showed a linear regime between 0.01 and 2% with the gel yielding at 7% to give liquid-like behavior ($G'' > G'$, Figure S4). The gel exhibited rapid self-healing[61] behavior with little loss in gel strength when the strain was repeatedly relaxed from 200 to 0.1% (Figure 2) as observed for other polymeric hydrogels cross-linked through coordination to simple metal complexes.[44] This effect was also observed in the bulk gel when two pieces of freshly cut gel were brought back together and the self-healing process occurred instantaneously, allowing the healed hydrogel to support its own weight (Figure S5). Scanning electron microscopy (SEM) of freeze-dried gel samples revealed a hierarchical network of pores ranging in size from 100 nm to 100 μm (Figure S6).

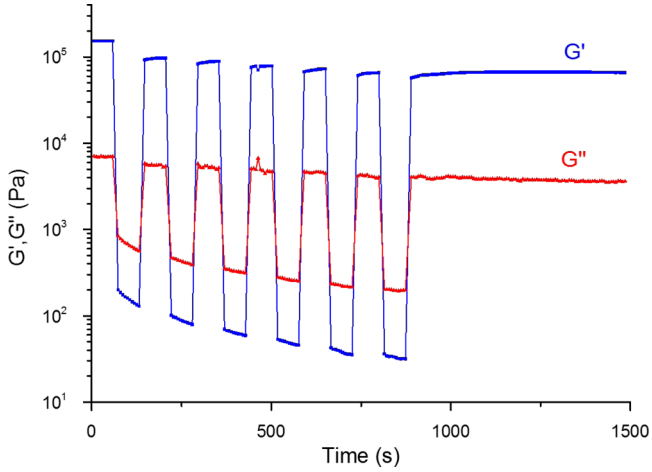

Figure 2. Rheological data highlighting the self-healing behavior of a 15 wt % gel of cage **2**. The gel was subject to alternating 60 s cycles of 0.1% then 200% oscillatory strain. The values for the elastic modulus G' (blue) and storage modulus G'' (red) are plotted. Measurements were taken at 25 °C with a fixed frequency of 10 rad/s.

The concentration of gel-forming subcomponents was found to affect the stability of the hydrogels (Supporting Information Section 1.3). When 10 wt % of the components of cage **2** were mixed, gelation was slowed, requiring 5 min for the aqueous solution to become immobile upon inversion. When 5 wt % of building blocks were used, only viscous purple solutions were observed, with no evidence of gel formation. When 15 wt % samples were prepared in which 4-aminophenyl-2-sulfonic acid (12 equiv) was used in place of 4,4′-diaminobiphenyl-2,2′-disulfonic acid (6 equiv), no gelation was observed and only a viscous purple solution was obtained. These building blocks would be expected to lead to the formation of 3-fold cross-links around mononuclear iron(II)-tris(pyridylimine) centers, but we infer that a higher degree of cross-linking is required to form a stable hydrogel. The relatively high concentration of gel-forming subcomponents required to form stable gels compared to related hydrogelators is attributed to the use of short polymer chains. This high concentration is desirable for providing a high loading of cages within the gels for use in guest binding.

DOI: 10.1021/jacs.5b05507
J. Am. Chem. Soc. 2015, 137, 9722–9729

In order to investigate the dynamic nature of the hydrogel, a vial containing a 5 wt % solution of cage complex **2** was freeze-dried, resulting in a fibrous structure such as would be expected for a xerogel (Figure S2). The addition of a third of the original volume of water to yield a 15 wt % mixture initially resulted in a fluid solution; however, after 48 h this solution had formed a hydrogel which was stable to inversion. Similarly, the layering of 1.65 mL of deionized water on top of a freshly formed 15 wt % hydrogel (0.25 mL) resulted in gradual swelling, leading to breakdown of the gel and the formation of a purple solution overnight. However, if the hydrogel was allowed to set at room temperature for one month prior to wetting, the gel exhibited long-term stability, with little leaching of colored cage complex into the supernatant.

Upon the basis of these observations, we hypothesize that the 2-formylpyridine subcomponents attached to the termini of the short PEG chain can either cross-link between separate cages (*inter*) or loop back between attachment points on the same cage (*intra*). At higher concentrations (15 wt %), there are sufficient *inter*-cage spanning PEG chains to form a rigid gel matrix. However, at lower concentrations (5 wt %), the cross-link density is insufficient to form a stable network. When the 5 wt % solution was concentrated by freeze-drying and reconstitution, the dynamic nature of the linkages allowed rearrangement from an *intra*- to *inter*-cage cross-linked system, resulting in hydrogel formation. Similarly, the 15 wt % hydrogel continues to transform over time to form a more highly cross-linked network, which is better able to resist swelling upon hydration.

Cage Formation and Guest Binding. In order to monitor cage formation and guest binding in the hydrogels, a discrete model cage complex (**3**) was prepared using monoaldehyde **C**, a 2-formylpyridine grafted with a short, monofunctionalized PEG chain (Supporting Information Section 2.1). When cage **3** was prepared from **C** (Figure 1), ^{1}H NMR spectra collected just after the cage precursors were mixed showed a single set of broad resonances that sharpened over several days (Figures S8, S11). Diffusion ordered spectroscopy (DOSY) was consistent with these signals belonging to a single species (Figure S9), and confirmation of the M_4L_6 metal−ligand stoichiometry was provided by high-resolution mass spectrometry (Figure S10). The characterization data for cage **3** correspond well to those for the closely related tetrahedral cage **1**, prepared from the parent 2-formylpyridine **A**. Further, the resonances in the aromatic region of the ^{1}H NMR spectrum of cage **3** correlated well with the broad resonances observed for 5 wt % mixtures of cage complex **2** (Figure S12). The ^{1}H NMR spectrum of a 15 wt % hydrogel of cage complex **2** showed only broad resonances centered around 3.6 ppm, corresponding to the PEG chains (Figure S12).

^{19}F NMR spectroscopy was used to investigate the binding of fluorobenzene to cages in hydrogels of **2** (Figure 3). Fluorobenzene has previously been shown[62] to bind within cage **1** with a binding constant (K_a) of 6.1×10^2 M^{-1} and rate constant for guest uptake (k_{in}) of 2.21×10^{-1} M^{-1} s^{-1}. When fluorobenzene (8 equiv) was added to an aqueous solution of model cage **3** (5.6 mM), a new resonance was observed at −106.6 ppm, alongside that of free fluorobenzene (−113.6 ppm). The new resonance was attributed to encapsulation inside **3** (Figures 3a, S13). A new resonance was clearly observed in 5 wt % solutions of cage complex **2** (Figure 3b). When 15 wt % hydrogels of **2** were prepared in the presence of fluorobenzene (Supporting Information Section 2.3), initially

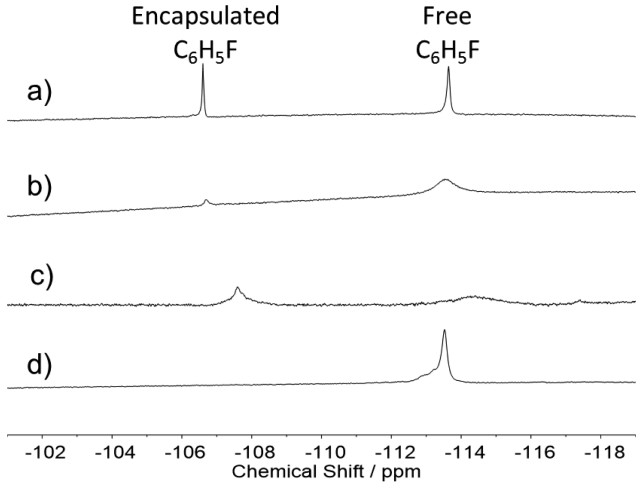

Figure 3. ^{19}F NMR spectra showing encapsulation of fluorobenzene in (a) cage **3**, (b) 5 wt % solution of cage complex **2**, (c) 15 wt % hydrogel of cage complex **2**, (d) a 15 wt % mixture of the subcomponents of **2** with 4-aminophenyl-2-sulfonic acid used in place of the diamine.

no new resonance was observed (Figure S13−S14) and there was considerable broadening of the free fluorobenzene resonance. However, when the sample was analyzed after 7 days, a new resonance corresponding to encapsulated fluorobenzene was observed. Encapsulation was observed most clearly when excess fluorobenzene was diffused into a hydrogel which had been allowed to set for 1 month (Figure 3c). In contrast, no resonances were observed at this chemical shift value when the mononuclear complex was prepared instead of the cage using a solution of 4-aminophenyl-2-sulfonic acid in place of the diamine (Figure 3d).

Guest Release Studies. Studies were undertaken to differentiate the behavior of molecules that were encapsulated within cage cavities from those that were entrained within gel pores. Benzene and furan were selected as UV-active guests known for strong, fast binding within **1**, with binding constants of 3.0×10^3 M^{-1} and 8.3×10^3 M^{-1} and rate constants for guest uptake of 1.58×10^{-1} M^{-1} s^{-1} and 2.1 ± 0.3 M^{-1} s^{-1}, respectively.[62] Anisole shows no binding to **1** so was selected as a nonguest control.

Six HPLC vials (2 mL) were prepared in identical fashion. Into each vial was added a 15 wt % aqueous solution of the building blocks of **2** (0.25 mL). The vial was tightly sealed and allowed to set for 1 month, in order to maximize gel stability. Each sample was then freeze-dried and swollen with 0.25 mL of an aqueous mixture containing a 1:1 solution of benzene and anisole (5 mM each). After swelling for 1 h, 1.65 mL of either pure water or aqueous furan solution (10 mM) was layered onto each gel, with each experiment being repeated three times. From each vial, 10 μL aliquots were extracted at set time intervals using an HPLC liquid-handling robot. Reference samples formed using 0.25 mL of benzene/anisole solution in water, diluted with either 1.65 mL of water or aqueous furan solution (10 mM), were treated in the same way.

HPLC was used to separate benzene and anisole from furan and the small amounts of the purple cage-complex that leached into the supernatant layer over the course of the experiment. The absorption of the eluent at 210 nm was measured using a UV−visible detector and the concentration of the benzene and anisole at each time point was calculated. A detailed description

DOI: 10.1021/jacs.5b05507
J. Am. Chem. Soc. 2015, 137, 9722−9729

of the protocols used and data obtained are included in Section 3 of the Supporting Information.

Figure 4a shows a plot of the average concentration of benzene (B) and anisole (A) released into the solution above the gel over time, in either the absence or presence of furan (F). When water was layered on top of the gels, the concentration of anisole released into solution (green square) gradually increased over 3 h to a concentration of 0.54 mM, whereas the concentration of benzene (red circle) increased only to 0.14 mM. After 7 h, 1.0 μL of furan was injected into the samples. This resulted in an increase in the concentration of benzene in the solution, which leveled off at 0.26 mM after 22 h (+18 h).

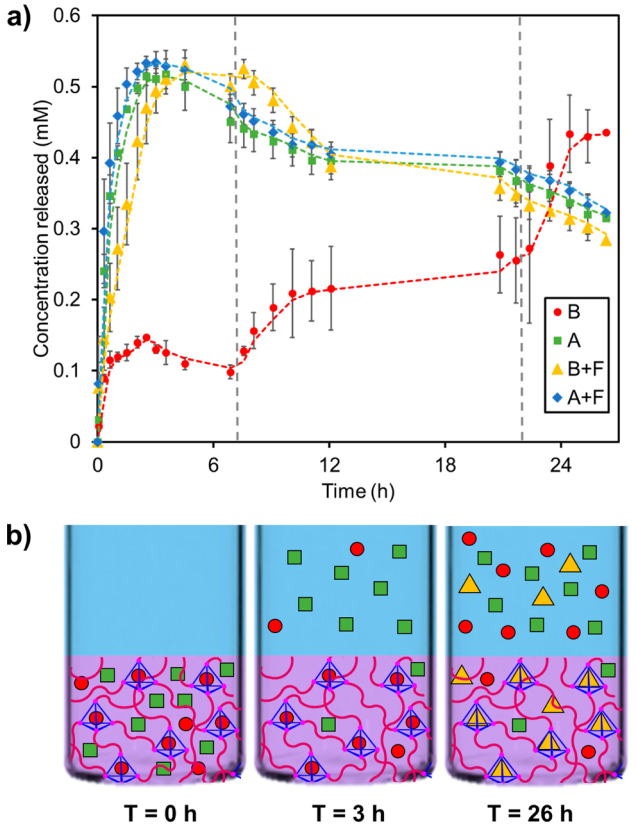

Figure 4. (a) Plot showing the release profiles of benzene (B) and anisole (A) in the presence or absence of the competing guest furan (F). Error bars show estimated standard deviations based on the three repeats of each sample, guidelines trace the two-point moving average. Furan was injected into nonfuran-containing samples at the times indicated by the vertical gray dashed lines. (b) Scheme contrasting the role of cages in moderating the release of cage-bound benzene (red circles) with unbound anisole (green squares) as the experiment progressed; furan (yellow triangles) acts as a competing guest for the cage, triggering the release of benzene.

Injection of a further 1.8 μL of furan resulted in a further increase in the concentration of benzene leveling off at 0.43 mM after 26 h. No corresponding increase in the concentration of anisole was observed, only a gradual decrease in concentration over time. This was attributed to evaporation of the anisole during measurements, as was also observed in control experiments where no gel was present (Figure S22–S23).

The samples to which an aqueous furan solution was added at the start of the experiment showed increases in both the concentration of benzene (yellow triangle) and anisole (blue diamond) to maxima of 0.52 and 0.53 mM, respectively, close to the initial values of benzene and anisole in the control solutions (0.48 and 0.63 mM, respectively, Figures S22–S23). The time taken to reach this concentration was on average slightly longer in the case of the benzene (4.5 h) than for the anisole (3 h). These samples were unaffected by subsequent injections with water, added to emulate the effects of the furan injection program. The anisole release profiles were in good agreement for both the addition of water and furan solutions, indicating that the presence of furan had no effect on the rate of release of anisole, in contrast to the different profiles observed for benzene.

Figure 4b shows in schematic form what we infer to happen in the differing cases of anisole and benzene. At the start of the experiment, the gels are loaded with both anisole and benzene, with benzene occupying both the cavities of the cages and surrounding gel pores, whereas anisole can only occupy the pores (Figure 4b, left). The layering of water on top of the gel results in the diffusion of anisole and benzene from the gel and into the supernatant. After 3 h, anisole becomes distributed between the solution and pores of the gel and is unaffected by the presence of the competing guest, furan. However, a large proportion of the benzene remains trapped within the cages of the gel (Figure 4b, center). Upon the addition of excess furan, which competes with benzene to bind within **1**,[31] guest exchange results in the release of benzene into solution (Figure 4b, right). These experiments demonstrate how the two different kinds of space may be accessed orthogonally, using different stimuli. It is possible to release selectively either the guests in the gel pores, or the gel-pore guests together with the cage-bound guests. Releasing the cage-bound guests while leaving the gel-pore guests intact, however, appears impractical given the looser binding of the latter.

Release experiments were also conducted using gels that had been formed using aqueous solutions saturated with benzene prior to freeze-drying (Supporting Information Section 3.4). Interestingly, while the release profiles were in good agreement with those observed in Figure 4, the final concentration of benzene in solution was considerably greater. A benzene concentration of 0.13 mM was observed, double the 0.066 mM observed in cases where deionized water was used to form the initial gels. This indicates that the benzene is retained within the cages during lyophilization, as has previously been reported with cyclohexane for cage **1**.[58] No retention of anisole was observed for gels prepared in the same way.

Triggered Release from Hydrogel Microparticles. In order to further investigate the properties of the metal–organic cage cross-linked hydrogels, we employed droplet-based microfluidics to fabricate hydrogel microparticles with high monodispersity and uniform composition.[42,43,63] Imaging of the microparticles by transmission and fluorescence microscopy allowed for visualization of gel properties, stimuli-responsive behavior and guest-release profiles.

Aqueous microdroplets were generated in a single step as an emulsion in oil within a polydimethylsiloxane (PDMS) microfluidic device. This device consisted of two aqueous channels intersecting with perpendicular oil flows at a single hydrophobic flow-focusing junction, as shown in Figures 5a and S24–25. At this junction, shear forces result in the formation of a microemulsion of monodisperse water-in-oil droplets (Supporting Information Video 1). In this work the continuous phase was the perfluorinated oil, Fluorinert FC-40 (3M), with 2 wt % perfluorinated surfactant (XL-01-171, Sphere Fluidics). A

DOI: 10.1021/jacs.5b05507
J. Am. Chem. Soc. 2015, 137, 9722–9729

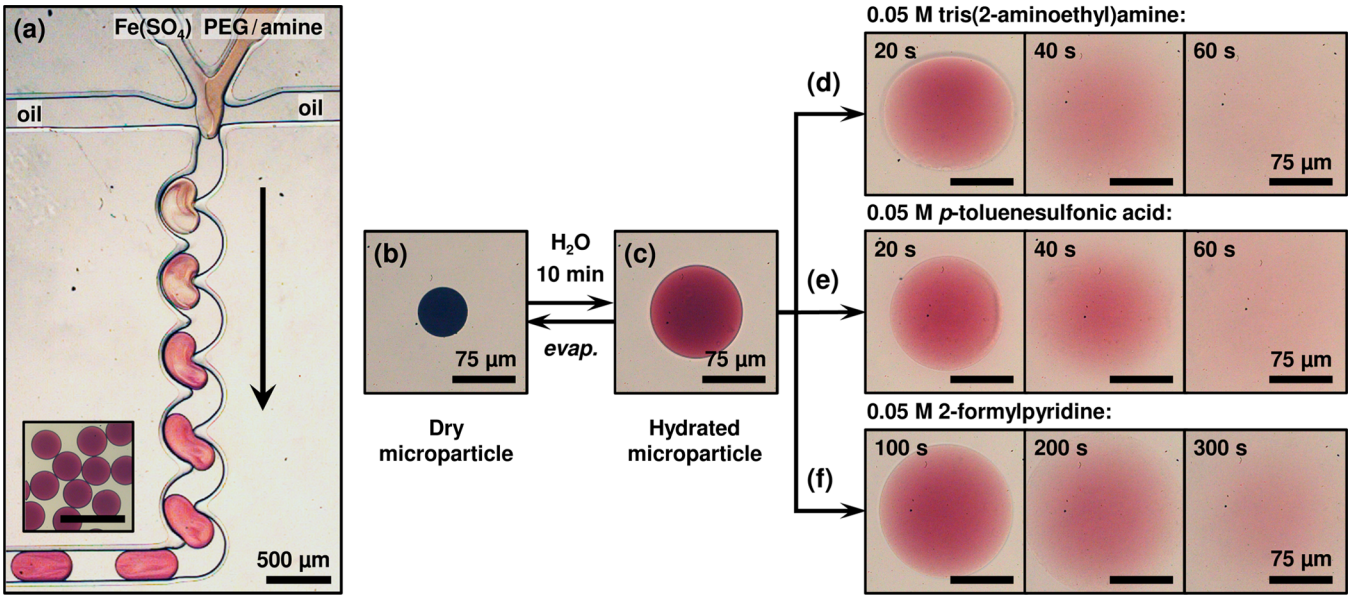

Figure 5. (a) Transmission optical micrograph of the generation of monodisperse water-in-oil microdroplets at a 200 μm microfluidic flow-focusing junction; subsequent in-droplet mixing of the two aqueous flows results in the formation of purple hydrogel microparticles. Inset: the resultant hydrogel microparticles upon exiting the microfluidic network. Scale bars are 500 μm. (b, c) The dry microparticles can be reversibly swollen upon addition of water (10 min). (d–f) Disassembly of the hydrogel microparticle can be triggered by addition of (d) tris(2-aminoethyl)amine, (e) *p*-toluenesulfonic acid or (f) 2-formylpyridine. Scale bars are 75 μm.

detailed description of device fabrication and droplet generation is included in the Experimental Section and Supporting Information (Section 4).

Microdroplets were prepared from a 1:1 flow of aqueous precursor solutions, with composition corresponding to 15 wt % solution of **2** in the mixed droplet. The cage-forming subcomponents were split between the two aqueous channels, with an aqueous solution of iron(II) sulfate combined with a solution containing the organic cage-forming subcomponents into a single laminar flow immediately prior to microdroplet generation. Rapid mixing of these cage-forming components within the droplet (accelerated through use of a winding channel) gave rise to the characteristic purple color observed in bulk preparations. Upon exiting the microbore tubing (<30 s) gelation had already occurred as evidenced by the presence of irregularities or surface "dents" from impact with, e.g. other microparticles, and the retention of aspherical shapes when the droplet diameter exceeded the channel cross section (Figure S26).

The newly formed hydrogel microparticles were deposited on to a fluorinated glass slide, and the evaporation of water from the particles under ambient conditions monitored. It was observed that upon evaporation, microparticles contracted to ~50% of their original diameter with a corresponding increase in opacity, while retaining their original shape (Figures 5b and S26–27). The dried microparticles could be rehydrated by adding deionized water. The gel was observed to swell rapidly over 1 min, with the original diameter restored within 10 min (Figure 5c, S28). Beyond this point the gel microparticle continued to swell over the course of an hour, reaching 150% of the original diameter; however it retained a defined boundary indicating that dissolution was not occurring. Upon removal of the surrounding media, the microparticles could be reproducibly dried back to the initial collapsed state, even when the process of swelling and deswelling in water was repeated five times (Figure S29). Control experiments in which only one of the two gel-forming solutions was present in the microdroplet resulted in microparticles that immediately dissolved upon addition of water (Figure S30).

Microdroplets were similarly generated containing 5.0, 7.5, and 10 wt % of gel forming subcomponents, with all loadings resulting in the formation of purple microdroplets. However, for 5.0 and 7.5 wt % loading, the cross-linking density within the droplet was not sufficient to form a gel microparticle; instead gelation occurred upon evaporative concentration of the microdroplet, yielding a collapsed gel disk (Figure S31). Upon rehydration, this "disk" was observed to gradually dissolve into solution over a period of 10 min. In contrast, samples that had been stored for 10 days behaved similarly to 15 wt % gel samples upon rehydration, with the microparticles reversibly swelling in deionized water (Figure S31c). This behavior correlates with the structural reconfiguration inferred in the bulk-phase post-freeze-drying.

Cage **1** has been shown to respond to a variety of stimuli, including acid and the addition of competing amine and aldehyde subcomponents, allowing for triggered release of cargo from inside the cage cavities.[58] Figure 5d–f shows that disassembly of the cage can be used to trigger disassembly of the gel microparticles. Here, addition of 0.1 M aqueous solution of either tris(2-aminoethyl)amine, *p*-toluenesulfonic acid or 2-formylpyridine to a hydrated gel microparticle resulted in disassembly of the cage, with the gel observed to disperse into solution. This process took less than 1 min for both acid and amine triggers; however, the competing aldehyde was noticeably slower, taking up to 5 min for the microparticle to disperse (Figure S32). Rapid disassembly was similarly observed upon hydrating dry microparticles directly with the above solutions (Figure S33). In all cases, the increase in particle size and uniform loss of color indicates that dissolution of the microparticles occurred by swelling, rather than an erosion-based mechanism.[10] Different colors were observed in the residue left following cage disassembly using different chemical

DOI: 10.1021/jacs.5b05507
J. Am. Chem. Soc. 2015, 137, 9722–9729

triggers, which correlated with the expected disassembly products (Figure S34).

The retention and release of cargo from the hydrogel microparticles by diffusion and in response to chemical stimuli was investigated by fluorescence microscopy. As the cavity of the cage in gels of **2** is too small to host suitable fluorescent tracers, the macromolecular cargo, fluorescein isothiocyanate-dextran (FD, 70−500 kDa, 3.0 mg mL^{-1}) was employed. Microdroplets were generated using a three-input microfluidic device that allowed for introduction of cargo independently to gel-forming components, as shown in Figure S35. Following initial swelling for 10 min, diffusion of fluorescent cargo from microparticles containing low molecular weight FD (<150 kDa, Figure S36) into the surrounding media was observed. In contrast, the microparticles were impermeable to FITC-dextran with higher molecular weights (250 and 500 kDa) as shown by the localization of fluorescence within the hydrated gel microparticle (Figure S36). Based on the corresponding Stokes radii of the FD cargoes, we infer these microparticles to have hydrated pore sizes 17−21 nm in diameter. SEM images of the freeze-dried microdroplets (Supporting Information Section 4.6) show a hierarchical network of pores as observed in the bulk gel. It should be noted that it was not possible to resolve the fine structure of the gels due to the need to coat the samples to prevent surface charging on exposure to the electron beam.

As shown in Figure 6, the hydration of microparticles loaded with 500 kDa FD (1 mg/mL) in deionized water resulted in swelling, but little loss of cargo. The rings in the fluorescent micrographs are attributed to strong absorbance by the cage at the emitted wavelength rather than the distribution of fluorescent cargo within the microparticles. The subsequent addition of *p*-toluenesulfonic acid (to make an overall concentration of 0.05 M) was then used to trigger microparticle disassembly, with corresponding release of FD cargo into the surrounding media. This process proceeded approximately six times more slowly than for unloaded microparticles (as shown previously in Figure 5) with sustained release of cargo observed after 2 min, and a further 4 min required for the microparticles to completely disassemble releasing their cargo into the surrounding media. This delay was attributed to the FITC-dextran cargo within the gel pores inhibiting access of the acid to the cage-cross-links, slowing the rate of disassembly.

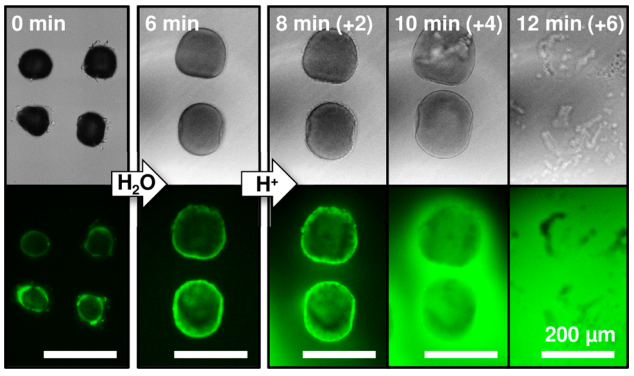

Figure 6. Transmission optical (top) and fluorescence (bottom) micrographs of hydrogel microparticles containing FITC-dextran macromolecular cargo (500 kDa, 1.0 mg mL^{-1}). Upon hydration in water the microparticles swell, but retain cargo. Subsequent addition of 0.1 M *p*-toluenesulfonic acid results in disassembly of the hydrogel with corresponding release of the fluorescent cargo into the surrounding media. Scale bars are 200 μm.

CONCLUSION

Metal−organic cage-cross-linked hydrogels combine the mesoscopic pores of polymeric supramolecular gels with the well-defined guest-binding properties of metal−organic cages. In this work, we have shown how the two internal phases present within the gels allow closely related small molecules to be released at different rates and in response to competing guests, depending on whether they are selectively encapsulated within the inner phases of the cages. The rapid self-assembly of hydrogels upon mixing of solutions of subcomponents with metal ions at room temperature allowed for the formation of monodisperse hydrogel microparticles through the use of droplet based microfluidics. These microparticles provided a visual demonstration of the dynamic behavior of the gels in response to a variety of stimuli and allowed for the triggered release of macromolecular cargo.

Other hydro- and organo-gels incorporating different metal−organic or organic cage[64] moieties with internal cavities capable of binding guests, such as drug molecules, fragrances or pesticides, may be accessible using the methods here presented. The incorporation of cage-cross-links expands the range of host−guest chemistry that can be used in affinity-based gel delivery systems compared to those based on macrocycles,[10] complementing what may be accomplished using other complex controlled delivery systems based on porous materials.[65−70] The host−guest properties of cages have also been exploited in a variety of other ways, for example, as homogeneous catalysts[25−27] and sensors[26] and incorporating cages into the gel phase opens up the possibility of undertaking these same processes heterogeneously, allowing for the separation of products and recovery of the cages. Metal−organic cage-cross-linked polymers therefore represent a platform for the development of new multifunctional materials.

EXPERIMENTAL SECTION

General Methods. Commercial solvents and reagents were used without further purification. All reactions were carried out in dry glassware with a nitrogen overpressure. NMR spectra were recorded on a Bruker Advance DPX 400 or Bruker Advance Cryo 500 spectrometer. Chemical shifts for ^{1}H, ^{13}C, and ^{19}F are reported in ppm on the δ scale; ^{1}H and ^{13}C were referenced to the residual solvent peak, and ^{19}F was referenced to C_6F_6 at δ= −163 ppm. All coupling constants are reported in Hz. Electrospray Ionization mass spectra (ESI-MS) for the ligands were obtained on a Micromass Quattro LC infused from a Harvard Syringe Pump. The mass spectrometric service for cage **3** were performed by the National Mass Spectrometry Facility at Swansea University using a Thermo Scientific LTQ Orbitrap XL mass spectrometer in negative ionization mode. Samples were dissolved in water, diluted 1:100 with methanol and infused with an Advion TriVersa NanoMate at a rate of 0.25 μL min^{-1}. Elemental analyses were obtained on an Exeter Analytical CE-440 Elemental Analyzer. Rheology experiments were performed using a TA Instruments Advanced Rheometer 2000 equipped with a Peltier heating plate. Scanning Electron Microscopy (SEM) was carried out on a FEI Nova NanoSEM with accelerating voltages of 2−5 keV.

Synthesis of Dialdehyde B. To a round-bottom flask was added cesium carbonate (560.9 mg, 1.72 mmol), polyethylene glycol (RMM = 1000 g mol^{-1}, 208.9 mg, 0.21 mmol) and dry dimethylformamide (25 mL). The reaction mixture was stirred at 110 °C for 1 h. 5-Fluoro-2-formylpyridine (130.9 mg, 1.05 mmol) was added and the reaction was stirred for a further 48 h at 100 °C. The DMF was removed under reduced pressure and the resultant brown oil was dissolved in 50 mL

DOI: 10.1021/jacs.5b05507
J. Am. Chem. Soc. 2015, 137, 9722−9729

DCM, to which 1 M $HCl_{(aq.)}$ (10 mL) was added and the mixture stirred for 10 min. Once complete, 4.0 M $NaOH_{(aq.)}$ (30 mL) was added and the organic layer extracted under basic conditions. The organic layer was dried with $MgSO_4$ and concentrated under reduced pressure to afford a brown oil. Excess 5-fluoropyridine could be removed by repeated washing of the oil with diethyl ether. The oil was further dried under high vacuum at 50 °C to give dialdehyde **B** (200 mg, 80%) and stored in a freezer at −20 °C until use. ^{1}H NMR (500 MHz, $CDCl_3$) δ/ppm 9.19 (1H, s, CHO), 8.48 (1H, d, J 2.8, ArH), 7.99 (1H, d, 8.8 Hz, ArH), 7.36 (1H, dd, J 8.8, 2.8, ArH), 4.30 (2H, t, J 4.6, $ArOCH_2$), 3.91 (2H, t, J 4.8, $ArOCH_2CH_2$), 3.78−3.62 (40 H, m, OCH_2). ESI-MS (MeOH): m/z 472.6, 516.2, 538.2, 560.3, 582.3, 604.3, 626.3, 648.3, 670.3, 692.4, 714.4 ($[M + 2Na - C_6H_3NO]^{2+}$ for n = 18−29), 955.5, 999.5, 1043.5, 1087.5, 1131.5, 1175.6, 1219.6, 1263.6, 1307.7, 1351.7, 1395.6 ($[M + 2Na]^+$ for n = 16−26). Elemental calculated for $C_{56}H_{96}N_2O_{25}$: C, 56.17; H, 8.08; N, 2.34. Found: C, 57.06; H, 8.12; N, 2.27.

Synthesis of Monoaldehyde C. To a round-bottom flask was added cesium carbonate (500.9 mg, 1.54 mmol), triethylene glycol monomethyl ether (100.97 mg, 0.61 mmol) and dry dimethylformamide (25 mL). The reaction mixture was stirred at 100 °C for 1 h. 5-Fluoro-2-formylpyridine (105.8 mg, 0.85 mmol) was added and the reaction was stirred for a further 18 h at 100 °C. The DMF was removed under reduced pressure and the resultant brown oil was dissolved in 50 mL DCM, to which 1 M $HCl_{(aq.)}$ (10 mL) was added and the mixture stirred for 10 min. 4.0 M NaOH (30 mL) was added and the organic layer extracted under basic conditions. The organic layer was dried with $MgSO_4$ and concentrated under reduced pressure to afford monoaldehyde **C** as a brown oil (128 mg, 77%) and stored in a freezer at −20 °C until use. ^{1}H NMR (400 MHz, $CDCl_3$-d) δ/ppm 10.00 (s, 1H, CHO), 8.47 (d, J = 2.7 Hz, 1H, ArH), 7.96 (d, J = 8.7 Hz, 1H, ArH), 7.35 (dd, J = 8.6, 2.7 Hz, 1H, ArH), 4.33−4.22 (m, 2H, $ArOCH_2$), 3.96−3.90 (m, 2H, $ArOCH_2CH_2$), 3.78−3.53 (m, 8H, OCH_2), 3.39 (s, 3H, OCH_3). ESI-MS (MeOH): 165.08 (35%, $[M - C_6H_4NO]^+$), 165.08 (25%, $[M - C_6H_4NO + Na]^+$) 270.8 (100%, $[M + H]^+$). Elemental calculated for $C_{13}H_{19}NO_5$: C, 57.98; H, 7.11; N, 5.20. Found: C, 57.93; H, 7.14; N, 5.24.

Guest Release Study. The chemical composition of the supernatant in guest release studies was analyzed by reverse phase HPLC using a modular Agilent 1100 Series HPLC system composed of a HPLC high pressure binary pump, autosampler with injector programming capabilities, column oven with 6 μL heat exchanger and a Diode Array Detector with a semimicro flow cell to reduce peak dispersion.

Droplet-Based Microfluidics. Microfluidic devices were fabricated from PDMS via soft lithography. To render the channels fluorophilic they were immediately flushed with a 0.5% v/v solution of trichloro(1H,1H,2H,2H-perfluorooctyl)silane in Fluorinert FC-40 (3M). Aqueous microdroplets were generated in a single step as an emulsion in oil within the microfluidic device. This consisted of two aqueous channels intersecting with perpendicular oil flows at a single flow-focusing junction (200 × 80 μm). To generate microdroplets, the continuous oil phase and the discrete aqueous phase were injected into the microfluidic device via two syringe pumps (PHD 2000, Harvard Apparatus) with typical flow rates of AQ_{Fe} = AQ_{PEG} = 80 μL h^{-1} and Oil = 200 μL h^{-1}, giving rise to 220 μm diameter microdroplets (Figure 4a). Alternatively, a microfluidic device where three aqueous inputs intersected at a single flow-focusing junction (120 × 80 μm) was used to introduce cargo independently to gel-forming components. Here typical flow rates of AQ_{tot} = 200 μL h^{-1} and Oil = 100 μL h^{-1} gave rise to 200 μm diameter microdroplets (Figure S37). All aqueous solutions were prepared in deionized water (Millipore Milli-Q Gradient A10) ensuring a resistivity of >15 MΩ cm^{-1}.

Microparticles were imaged using a Vision Research Phantom Miro EX-4 fast camera with color interpolation, mounted to an Olympus IX-71 inverted microscope (10−64× objectives). Images were color corrected using Irfanview. The fluorescent label, fluorescein (ex: 488 nm, em: 500−535 nm) were used to track the location of macromolecular cargo (FD, 70−500 kDa) within the microdroplet. Fluorescence micrographs were obtained under illumination from a coolLED pE-300white (blue waveband, 450 mW) lamp and imaged with an Olympus IX-81 inverted microscope (Prior proscan II automated stage) mounted with an Andor iXonEM+ DU 897 EMCCD camera, controlled via a PC running custom LabVIEW 2013 software. Images were recolored with ImageJ.

■ ASSOCIATED CONTENT

Supporting Information

Detailed experimental procedures and further characterization for the synthesis of aldehydes **B** and **C**, the corresponding cage complexes, guest binding and release studies and microdroplet work (Figures S1−38). The Supporting Information is available free of charge on the ACS Publications website at DOI: 10.1021/jacs.5b05507.

■ AUTHOR INFORMATION

Corresponding Author

*jrn34@cam.ac.uk

Notes

The authors declare no competing financial interest.

■ ACKNOWLEDGMENTS

This work was supported by the European Research Council (259352). We thank the Cambridge Chemistry NMR service for experimental assistance, and the EPSRC Mass Spectrometry Service at Swansea for carrying out high-resolution mass spectrometry. AMB thanks the EPSRC for funding. NK thanks the JSPS for a Research Fellowship for Young Scientists.

■ REFERENCES

(1) Huang, X.; Brazel, C. S. *J. Controlled Release* **2001**, *73*, 121.
(2) Uhrich, K. E.; Cannizzaro, S. M.; Langer, R. S.; Shakesheff, K. M. *Chem. Rev.* **1999**, *99*, 3181.
(3) Lin, C. C.; Anseth, K. S. *Pharm. Res.* **2009**, *26*, 631.
(4) Herrmann, A. *Angew. Chem., Int. Ed.* **2007**, *46*, 5836.
(5) Majeed, Z.; Ramli, N. K.; Mansor, N.; Man, Z. *Rev. Chem. Eng.* **2015**, *31*, 69.
(6) De Cock, L. J.; De Koker, S.; De Geest, B. G.; Grooten, J.; Vervaet, C.; Remon, J. P.; Sukhorukov, G. B.; Antipina, M. N. *Angew. Chem., Int. Ed.* **2010**, *49*, 6954.
(7) Duncanson, W. J.; Lin, T.; Abate, A. R.; Seiffert, S.; Shah, R. K.; Weitz, D. A. *Lab Chip* **2012**, *12*, 2135.
(8) Walker, S.; Oun, R.; McInnes, F. J.; Wheate, N. J. *Isr. J. Chem.* **2011**, *51*, 616.
(9) Vermonden, T.; Censi, R.; Hennink, W. E. *Chem. Rev.* **2012**, *112*, 2853.
(10) Wang, N. X.; von Recum, H. A. *Macromol. Biosci.* **2011**, *11*, 321.
(11) Concheiro, A.; Alvarez-Lorenzo, C. *Adv. Drug Delivery Rev.* **2013**, *65*, 1188.
(12) Vulic, K.; Pakulska, M. M.; Sonthalia, R.; Ramachandran, A.; Shoichet, M. S. *J. Controlled Release* **2015**, *197*, 69.
(13) Tranchemontagne, D. J. L.; Ni, Z.; O'Keeffe, M.; Yaghi, O. M. *Angew. Chem., Int. Ed.* **2008**, *47*, 5136.
(14) Löffler, S.; Lübben, J.; Krause, L.; Stalke, D.; Dittrich, B.; Clever, G. H. *J. Am. Chem. Soc.* **2015**, *137*, 1060.
(15) Han, M.; Engelhard, D. M.; Clever, G. H. *Chem. Soc. Rev.* **2014**, *43*, 1848.
(16) Sun, W. Y.; Yoshizawa, M.; Kusukawa, T.; Fujita, M. *Curr. Opin. Chem. Biol.* **2002**, *6*, 757.
(17) Cook, T. R.; Zheng, Y. R.; Stang, P. J. *Chem. Rev.* **2013**, *113*, 734.
(18) Yan, X. Z.; Cook, T. R.; Wang, P.; Huang, F. H.; Stang, P. J. *Nat. Chem.* **2015**, *7*, 342.

DOI: 10.1021/jacs.5b05507
J. Am. Chem. Soc. 2015, 137, 9722−9729

(19) Fontenot, S. A.; Cangelosi, V. M.; Pitt, M. A. W.; Sather, A. C.; Zakharov, L. N.; Berryman, O. B.; Johnson, D. W. *Dalton Trans.* **2011**, *40*, 12125.
(20) Kishi, N.; Akita, M.; Kamiya, M.; Hayashi, S.; Hsu, H.-F.; Yoshizawa, M. *J. Am. Chem. Soc.* **2013**, *135*, 12976.
(21) Joyce, L. A.; Shabbir, S. H.; Anslyn, E. V. *Chem. Soc. Rev.* **2010**, *39*, 3621.
(22) Qi, Z.; Heinrich, T.; Moorthy, S.; Schalley, C. A. *Chem. Soc. Rev.* **2015**, *44*, 515.
(23) Kishi, N.; Akita, M.; Yoshizawa, M. *Angew. Chem., Int. Ed.* **2014**, *53*, 3604.
(24) Cullen, W.; Turega, S.; Hunter, C. A.; Ward, M. D. *Chem. Sci.* **2015**, *6*, 625.
(25) Yoshizawa, M.; Klosterman, J. K.; Fujita, M. *Angew. Chem., Int. Ed.* **2009**, *48*, 3418.
(26) Ahmad, N.; Younus, H. A.; Chughtai, A. H.; Verpoort, F. *Chem. Soc. Rev.* **2015**, *44*, 9.
(27) Brown, C. J.; Toste, F. D.; Bergman, R. G.; Raymond, K. N. *Chem. Rev.* **2015**, *115*, 3012.
(28) Ronson, T. K.; Zarra, S.; Black, S. P.; Nitschke, J. R. *Chem. Commun.* **2013**, *49*, 2476.
(29) Nitschke, J. R. *Acc. Chem. Res.* **2007**, *40*, 103.
(30) Smulders, M. M. J.; Riddell, I. A.; Browne, C.; Nitschke, J. R. *Chem. Soc. Rev.* **2013**, *42*, 1728.
(31) Ji, Q.; Lirag, R. C.; Miljanic, O. S. *Chem. Soc. Rev.* **2014**, *43*, 1873.
(32) Appel, E. A.; del Barrio, J.; Loh, X. J.; Scherman, O. A. *Chem. Soc. Rev.* **2012**, *41*, 6195.
(33) Rossow, T.; Hackelbusch, S.; van Assenbergh, P.; Seiffert, S. *Polym. Chem.* **2013**, *4*, 2515.
(34) Dong, R. J.; Zhou, Y. F.; Huang, X. H.; Zhu, X. Y.; Lu, Y. F.; Shen, J. *Adv. Mater.* **2015**, *27*, 498.
(35) Vulic, K.; Shoichet, M. S. *Biomacromolecules* **2014**, *15*, 3867.
(36) Foster, J. A.; Piepenbrock, M. O. M.; Lloyd, G. O.; Clarke, N.; Howard, J. A. K.; Steed, J. W. *Nat. Chem.* **2010**, *2*, 1037.
(37) Hirst, A. R.; Escuder, B.; Miravet, J. F.; Smith, D. K. *Angew. Chem., Int. Ed.* **2008**, *47*, 8002.
(38) Qi, Z.; Schalley, C. A. *Acc. Chem. Res.* **2014**, *47*, 2222.
(39) Rossow, T.; Bayer, S.; Albrecht, R.; Tzschucke, C. C.; Seiffert, S. *Macromol. Rapid Commun.* **2013**, *34*, 1401.
(40) Rossow, T.; Heyman, J. A.; Ehrlicher, A. J.; Langhoff, A.; Weitz, D. A.; Haag, R.; Seiffert, S. *J. Am. Chem. Soc.* **2012**, *134*, 4983.
(41) Wang, J.-T.; Wang, J.; Han, J.-J. *Small* **2011**, *7*, 1728.
(42) Tumarkin, E.; Kumacheva, E. *Chem. Soc. Rev.* **2009**, *38*, 2161.
(43) Theberge, A. B.; Courtois, F.; Schaerli, Y.; Fischlechner, M.; Abell, C.; Hollfelder, F.; Huck, W. T. S. *Angew. Chem., Int. Ed.* **2010**, *49*, 5846.
(44) Brassinne, J.; Fustin, C. A.; Gohy, J. F. *J. Inorg. Organomet. Polym. Mater.* **2013**, *23*, 24.
(45) Su, X.; Aprahamian, I. *Chem. Soc. Rev.* **2014**, *43*, 1963.
(46) McDonald, K. P.; Qiao, B.; Twum, E. B.; Lee, S.; Gamache, P. J.; Chen, C.-H.; Yi, Y.; Flood, A. H. *Chem. Commun.* **2014**, *50*, 13285.
(47) Wojtecki, R. J.; Meador, M. A.; Rowan, S. J. *Nat. Mater.* **2011**, *10*, 14.
(48) Krieg, E.; Shirman, E.; Weissman, H.; Shimoni, E.; Wolf, S. G.; Pinkas, I.; Rybtchinski, B. *J. Am. Chem. Soc.* **2009**, *131*, 14365.
(49) Harada, A.; Takashima, Y.; Nakahata, M. *Acc. Chem. Res.* **2014**, *47*, 2128.
(50) Foster, J. A.; Steed, J. W. *Angew. Chem., Int. Ed.* **2010**, *49*, 6718.
(51) Liu, Y.; Yang, H.; Wang, Z.; Zhang, X. *Chem. - Asian J.* **2013**, *8*, 1626.
(52) Dankers, P. Y. W.; Hermans, T. M.; Baughman, T. W.; Kamikawa, Y.; Kieltyka, R. E.; Bastings, M. M. C.; Janssen, H. M.; Sommerdijk, N. A. J. M.; Larsen, A.; van Luyn, M. J. A.; Bosman, A. W.; Popa, E. R.; Fytas, G.; Meijer, E. W. *Adv. Mater.* **2012**, *24*, 2703.
(53) Guvendiren, M.; Lu, H. D.; Burdick, J. A. *Soft Matter* **2012**, *8*, 260.
(54) Sun, Z. F.; Huang, Q. Y.; He, T.; Li, Z. Y.; Zhang, Y.; Yi, L. Z. *ChemPhysChem* **2014**, *15*, 2421.
(55) Bunzen, H.; Nonappa; Kalenius, E.; Hietala, S.; Kolehmainen, E. *Chem. - Eur. J.* **2013**, *19*, 12978.
(56) de Hatten, X.; Bell, N.; Yufa, N.; Christmann, G.; Nitschke, J. R. *J. Am. Chem. Soc.* **2011**, *133*, 3158.
(57) Asil, D.; Foster, J. A.; Patra, A.; de Hatten, X.; del Barrio, J.; Scherman, O. A.; Nitschke, J. R.; Friend, R. H. *Angew. Chem., Int. Ed.* **2014**, *53*, 8388.
(58) Mal, P.; Schultz, D.; Beyeh, K.; Rissanen, K.; Nitschke, J. R. *Angew. Chem., Int. Ed.* **2008**, *47*, 8297.
(59) Zarra, S.; Smulders, M. M. J.; Lefebvre, Q.; Clegg, J. K.; Nitschke, J. R. *Angew. Chem., Int. Ed.* **2012**, *51*, 6882.
(60) Ronson, T. K.; Giri, C.; Beyeh, N. K.; Minkkinen, A.; Topic, F.; Holstein, J. J.; Rissanen, K.; Nitschke, J. R. *Chem. - Eur. J.* **2013**, *19*, 3374.
(61) Li, L.; Yan, B.; Yang, J.; Chen, L.; Zeng, H. *Adv. Mater.* **2015**, *27*, 1294.
(62) Smulders, M. M. J.; Zarra, S.; Nitschke, J. R. *J. Am. Chem. Soc.* **2013**, *135*, 7039.
(63) Xu, S.; Nie, Z.; Seo, M.; Lewis, P.; Kumacheva, E.; Stone, H. A.; Garstecki, P.; Weibel, D. B.; Gitlin, I.; Whitesides, G. M. *Angew. Chem., Int. Ed.* **2005**, *44*, 724.
(64) Wang, Q.-Q.; Day, V. W.; Bowman-James, K. *Angew. Chem., Int. Ed.* **2012**, *51*, 2119.
(65) Wei, S.-C.; Pan, M.; Fan, Y.-Z.; Liu, H.; Zhang, J.; Su, C.-Y. *Chem. - Eur. J.* **2015**, *21*, 7418.
(66) Lülf, H.; Bertucci, A.; Septiadi, D.; Corradini, R.; De Cola, L. *Chem. - Eur. J.* **2014**, *20*, 10900.
(67) Coll, C.; Bernardos, A.; Martinez-Manez, R.; Sancenon, F. *Acc. Chem. Res.* **2013**, *46*, 339.
(68) O'Reilly, N.; Giri, N.; James, S. L. *Chem. - Eur. J.* **2007**, *13*, 3020.
(69) Horcajada, P.; Chalati, T.; Serre, C.; Gillet, B.; Sebrie, C.; Baati, T.; Eubank, J. F.; Heurtaux, D.; Clayette, P.; Kreuz, C.; Chang, J. S.; Hwang, Y. K.; Marsaud, V.; Bories, P. N.; Cynober, L.; Gil, S.; Férey, G.; Couvreur, P.; Gref, R. *Nat. Mater.* **2010**, *9*, 172.
(70) Mastalerz, M. *Chem. - Eur. J.* **2012**, *18*, 10082.

DOI: 10.1021/jacs.5b05507
J. Am. Chem. Soc. 2015, 137, 9722−9729